In: Radar Systems
Editor: Wen-Qin Wang
ISBN: 978-1-62417-872-6

Chapter 4

INTERPOLATION OF THE RADIAL VELOCITY DATA FROM COASTAL HF RADARS

Max Yaremchuk, [1] ***and Alexei Sentchev*** [2]
[1] Naval Research Laboratory, Stennis Space Center, MS, US
[2] Laboratoire d'Océanologie et Géosciences, Université du Littoral, France

Abstract

In recent years, monitoring nearshore surface currents became an important application of the high-frequency radar (HFR) technology. The Doppler shifts of backscattered radio signals from surface waves provide the surface velocity component in the direction of a HFR beam. These radial velocities observed by multiple (usually two) radars have to be combined/interpolated to produce the gridded vector field, which can be used in applications. In view of a relatively high (5-10 cm/s) HFR measurement errors of the radial velocities, interpolation algorithms which take into account additional constraints on the velocity field (such as those imposed by the coastlines and model dynamics) are of particular value.

In this chapter, recent developments in the radial velocity processing methods are reviewed. The topics include advanced optimal interpolation techniques, kinematically constrained Galerkin and the 2d variational interpolation methods, and the dynamically constrained assimilation of the HFR data using numerical models.

Accurate monitoring of the velocity field may suffer from occasional malfunction of a radar which causes a substantial data loss on a relatively short (3-30 hours) time interval. We examine performance of the gap-filling technique based on empirical orthogonal function analysis of the radial velocity observations and demonstrate its performance in tidally-driven coastal environments.

1. Introduction

The technology of monitoring near-coastal currents by High Frequency Radars (HFRs) has been rapidly developing in the past decade. HFR observations are now extensively used to study near-shore circulation under a large variety of environmental conditions (e.g., [40, 16, 17, 9, 43, 45, 11]) helping to solve many applied problems in the coastal regions. At present, the HFR surface current mapping technology is capable to provide surface velocity

maps in an area up to 200 km offshore, with space-time resolutions of 0.2-1 hour/1-10 km depending on the particular system and practical application.

An important question in dealing with HFR data is the problem of retrieving the 2d velocity vector maps from the velocity components measured along the radar beams. The most commonly used technique (e.g., [45]) is based upon local interpolation (LI) of the radial velocity data. The method is formulated as an unweighted least squares minimization problem and takes into account both measurement errors and the effect of geometric dilution of precision [10] associated with the angle between the HFR beams intersecting in a given grid cell. The LI method, being a particular case of the more general optimal interpolation (OI) technique, has been further improved by employing more sophisticated correlation functions [21, 22].

Another algorithm, which has been under development in recent years [26, 20] is the open-boundary modal analysis (OMA). This technique can be viewed as an extension of the normal mode analysis [13, 32] which, similarly to the later method of Park et al. [39], employs decomposition of a 2d vector field into divergent and rotational components. Apart from capability to avoid explicit specification of the poorly known error covariance, the OMA technique automatically takes into account the kinematic constraints imposed on the velocity field by the coastlines.

An alternative approach, proposed recently by Yaremchuk and Sentchev [51, 53], employs two-dimensional variational (2dVar) technique to map HFR radial velocity data on the gridded vector field. In contrast to the method of Park et al., [39], this algorithm does not require specification of a background velocity field and its covariance structure that may be lacking in many applications. Similar to OMA, the 2dVar method is non-local (the result of interpolation at a given grid point depends on all the observed radial velocities) and kinematically constrained (the interpolated velocity field is subject to constraints imposed by the coastlines). In addition, the 2dVar method [51] allows to impose constraints on the structure of the divergence and vorticity fields, that are important in practical applications, such as search and rescue, oil spill control etc.

Accuracy in the reconstruction of the surface velocity field measured by HFRs can be further improved by synthesis with other observations and with dynamical constraints provided by the numerical models. One of the earlier attempts of this kind was made by Lewis et al., [28], who employed HFR data to constrain wind stress forcing of a primitive-equation model. With subsequent development of the data assimilation (DA) techniques, the HFR data were widely used to constrain numerical models in the framework of both sequential [35, 36, 9] and 4dVar [19, 24] DA schemes. Although being more general, the dynamically constrained methods of HFR data interpolation are significantly more computationally expensive and often require a lot of preliminary tuning and quality control. For that reason, operational centers currently use more simple interpolation methods.

An obvious advantage of HFR observations is their availability in real time with nearly continuous temporal and spatial coverage fully compatible with the resolution of numerical models of coastal circulation. However, the back-scattered HFR signals suffer from to numerous distortions of artificial and natural origin. As a consequence, estimates of the along-beam sea surface velocities extracted from the Doppler shifts of the signals become unusable, resulting in numerous gaps in spatial coverage. These gaps may strongly degrade performance of the interpolation algorithms (e.g., [20]).

A natural way to fill these gaps is to take into account space-time correlations between the radial velocities. The aforementioned DA algorithms is the most straightforward and general approach. The underlying idea is to combine dynamical constraints of a model with the history of dense spatio-temporal coverage by HFRs to produce the "best" estimate of the surface velocity at a given time. This approach, however, has a number of drawbacks hindering its implementation for real-time HFR data analysis: Beyond a relatively high computational cost, the dynamically constrained DA schemes have a large number of free parameters whose statistics is poorly known. The most problematic among those are the open boundary conditions, which are the major contributors to slow convergence of the HFR DA schemes which typically involve lengthy open boundaries.

Although the 2d OI methods are computationally cheaper than the variational schemes involving dynamical information, they may perform poorly in the presence of large gaps in the data because information on the spatial structure of the velocity field within the gap is implicitly drawn from the idealized covariance function, which looses accuracy at large distances. A certain improvement of the covariance models can be obtained by considering their truncated expansions in the empirical orthogonal functions (EOFs), a technique successfully used in Kalman filtering (e.g., [49]) and variational data assimilation [14], [52]. The EOF-based estimates of the covariances rely upon time averaging and, therefore, may be successfully applied not only to model output but also to data sets with nearly continuous space-time coverage such as sea surface temperature (SST) or HFR data. Beckers and Rixen [7] proposed an iterative EOF-based technique for filling gaps in the gridded SST images, which was successfully applied in the Adriatic [1, 2]. Kondrashov and Ghil [23] developed the method further by including time correlations under the assumption of statistical stationarity of the observed fields. Yaremchuk and Sentchev [53] successfully applied this gap-filling (GF) technique to the HFR data.

In this chapter we give an overview of the radial velocity interpolation methods with a focus on the kinematically constrained 2d interpolation schemes and the GF techniques, that are likely to be introduced operationally in the near future.

The chapter is organized as follows: In the next section we describe the LI, OMA and 2dvar algorithms and compare their performance in the framework of numerical experiments with simulated and real data. In Section 3 we give an overview of the accumulated experience in the dynamically constrained interpolation of the HFR data and their synthesis with other observations. Section 4 describes applications of the HFR GF algorithm with both simulated and real data acquired in tidally-driven coastal environments.

2. Dynamically Unconstrained Interpolation Methods

The general approach discussed in this section can be classified as the two-dimensional OI, or spline interpolation [34]: The corresponding least-squares algorithms differ from each other by specifying either the covariance function or its inverse. In application to HFR data the OI algorithms were implemented using empirical error covariances deduced from "normal modes" [32], "open-boundary modes" [20] and the data [21], [22]. The spline formulation [51] defines the inverse covariance by the roughening operator which penalizes the grid-scale variability in the 2d velocity, divergence and vorticity fields.

2.1. Description of the Methodologies

2.1.1. Optimal Interpolation

In application to interpolation of the radial velocities v, the traditional OI approach is formulated as the following minimization problem: find the interpolated velocity field $\boldsymbol{u}(\boldsymbol{x})$ such, that given a set of n HFR velocity observations $v_i,\ i = 1,...,n$ around $\boldsymbol{x}$, the interpolation error variance ε^2 is minimized:

$$\langle \varepsilon^2 \rangle = \langle \sum_{i=1}^{n} w_i (v_i - \boldsymbol{u}(\boldsymbol{x}_i)\cdot \boldsymbol{r}_i)^2 \rangle \rightarrow \min_{\boldsymbol{u}} \tag{1}$$

Here angular brackets denote statistical average, $\boldsymbol{r}_i$ stand for the radar beam directions in the observation points and w_i are the weights derived from the statistics of $\boldsymbol{u}(\boldsymbol{x})$ (e.g., [30]). The approach requires a statistical model for the correlation tensor $\langle \boldsymbol{u}\boldsymbol{u}^{\mathrm{T}} \rangle$ of the interpolated field, which may not be readily available from observations. Therefore, in many practical applications, eq. (1) is simplified by selecting the grid which is coarse enough to contain at least two observation points from different radars within a given grid cell. By neglecting the decay of correlations within the cell, the problem can be reformulated locally (e.g., [45]): Find the velocity vector $\boldsymbol{u}$ at a given grid point such that deviations of its projections on the beam directions $\boldsymbol{r}_i$ at the surrounding observation points are minimized. In the most common case with only two radars illuminating a grid point, the solution is

$$u = (v_1 \cos\alpha_2 - v_2 \cos\alpha_1)/\sin(\alpha_1 - \alpha_2) \tag{2}$$

$$v = (v_2 \sin\alpha_1 - v_1 \sin\alpha_2)/\sin(\alpha_1 - \alpha_2) \tag{3}$$

where $v_{1,2}$ are the observed radial velocities and $\alpha_{1,2}$ denote angles between the coordinate axes and the beam directions $\boldsymbol{r}_{1,2}$ at the grid point. This local interpolation (unweighted least squares) method has been widely used in operational centers because of its robustness and simplicity. However, due to discontinuous correlation functions it often yields spurious values along baselines between HFR stations. Moreover, as it is seen from (2-3), the algorithm looses accuracy with the reduction of the angle $\alpha_1 - \alpha_2$ between the radar beams in the vicinity of the interpolated point, and it would not work at all with only one radar, or in the regions of sparse HFR coverage.

2.1.2. Normal Mode Analysis

Limitations imposed by the local nature of the LI algorithm can be formally overcome by the Galerkin methods which employ global basis functions covering the entire interpolation domain. The early technique of this type was proposed by Eremeev et al. [13] for interpolation of the sparsely sampled velocities. Later, Lipphardt et al [32] applied the technique to HFR observations. To perform the interpolation, the 2d velocity field is decomposed into divergent and rotational components defined by the velocity potential φ and the stream function ψ. The stream function and velocity potential are then expanded in a predetermined set of 2d functions (normal modes) with varying smoothness (eigenfunctions of the Laplacian operator Δ in the interpolation domain Ω). Expansion coefficients are then optimized to fit the data.

The normal mode method was further developed by Lekien and Coulliette [26], Kaplan and Lekien [20] who supplemented the Laplacian eigenfunctions by the additional expansion functions (open boundary modes). These functions were introduced to bring more realism near the open boundary, and were defined as solutions to the Poisson equation forced by the Dirichlet boundary conditions of variable smoothness. The algorithm is controlled by two free parameters: the spatial length scale L which defines the number of modes used for interpolation, and the regularization parameter κ which penalizes the amplitude of the modes.

An advantage of the OMA method is its ability to control spatial roughness by prescribing a limited number of the smoothest eigenfunctions for interpolation. Additionally, the method is capable to constrain the interpolation problem kinematically by taking into account the conditions imposed by the coastlines. However, the OMA method lacks flexibility in representing localized small-scale features as well as flow structures near open boundaries, where the rotational component of the velocity field is assumed to be tangent to the boundary. Besides, certain difficulties may arise when dealing with gappy data, especially when the horizontal size of a gap is larger than the minimal length scale resolved [20]. These drawbacks of the OMA technique may impose certain limitations on taking the full advantage of the HFR data whose spatial resolution strongly varies across the domain.

2.1.3. Variational Method

Interpolation of the HFR data with variational technique is more flexible, as it is not constrained by a predetermined set of functions. Instead, the interpolating functions in use (eigenvectors of the Hessian matrix) depend both on the shape of the coastline and spatial distribution of the data points. The latter feature (lacking in OMA) is especially useful in practice, because HFR data often have gaps in spatial coverage, and the issue of filling those gaps is important.

Another useful property of the 2dVar method is that, similar to LI, it operates in the velocity space, and thus requires less sophisticated operators for projection of the unknown gridded velocities on the radial components of the flow speed. This property provides better conditioning of the Hessian matrix, faster convergence of the minimization algorithm and improved computational efficiency.

The basic formulation of the 2dVar scheme [51, 53] is the following: Find the velocity field $\boldsymbol{u}(\boldsymbol{x})$ such, that the cost function

$$J = \frac{1}{2K}\sum_{k=1}^{K}\sigma_k^{-2}\left[(\hat{P}_k\boldsymbol{u})\boldsymbol{r}_k - v_k\right]^2 + \frac{1}{2A}\int_{\Omega}\left[W^d(\Delta\mathrm{div}\boldsymbol{u})^2 + W^c(\Delta\mathrm{curl}\boldsymbol{u})^2 + W^u(\Delta\boldsymbol{u})^2\right]d\Omega \to \min_{\boldsymbol{u}} \tag{4}$$

is minimized with respect to the grid point values $\boldsymbol{u}$ under the constraint $\boldsymbol{u}(\partial\Omega) = 0$. Here K is the number of HFR observations in Ω, $A = \int d\Omega$ and $\hat{P}_k$ is the local interpolation operator which projects the unknown velocity vectors onto the kth observation point from the apexes of the grid cell, enveloping that point. Factors σ_k^{-2}, W^d, W^c and W^u are the inverse error variances of the corresponding squared quantities, so that J could be treated as the argument of the Gaussian pdf $\mathcal{P}(\boldsymbol{u})$ defined on the $2M$-dimensional space of the gridded velocity fields $\boldsymbol{u}$: $\mathcal{P}(\boldsymbol{u}) \sim \exp[-J]$.

As it is seen from (4), regularization of the interpolation problem is performed by penalizing not only the grid-scale components of $\boldsymbol{u}$ (the last term), but also of its curl and

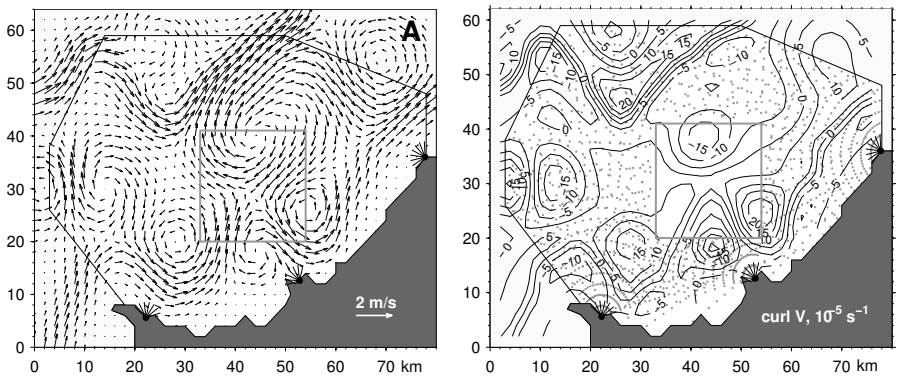

Figure 1. Setting of the numerical experiments: Left panel shows the "true" velocity field $\boldsymbol{u}^t$ which has nine eddy structures superimposed on two jets: one following the coastline and another located farther offshore. The right panel shows the vorticity field curl$\boldsymbol{u}^t$. Three coastal radars sample the radial velocities along beam directions binned at 2 km radial and 5° azimuthal resolution. Sampling points are shown by gray dots. Gray rectangle in the upper right panel envelops simulated gap in the HFR data. Radar positions are shown by black dots on the coastline. The interpolation domain and the coastline are similar to the ones used in [20] for OMA processing of HFR observations in the Bodega Bay. The coordinate system is rotated clockwise (north is on the right). Contour interval for vorticity is $5\cdot10^{-5}$ s^{-1}.

divergence (terms weighted by W^d and W^c). This is done in an attempt to retrieve the larger-scale components of div$\boldsymbol{u}$ and curl$\boldsymbol{u}$ that are important in applications.

2.2. Comparison of the Interpolation Techniques

Performance of the interpolation methods outlined in the previous section are compared using two complimentary techniques. First, the HFR data are simulated using a realistic geometry of the 3-radar experiment in the Bodega Bay conducted in spring and summer of 2003 (Fig. 1). In the second series real data acquired on July 30, 2003 in the Bodega Bay and offshore the coast of Brittany has been used.

2.2.1. Experiments with Simulated Data

Simulated data experiments are performed by varying the interpolation method (2dVar, LI and OMA) and coverage of the domain by observations (with and without the gap shown in the right panel of Figure 1). Within each series of experiments the noise level ν in the simulated observations was also varied: the radial velocities v_k^* observed at points $\boldsymbol{x}_k$ were defined by adding white noise w to projections of the true currents $\boldsymbol{u}^t$ on the beam directions $\boldsymbol{r}_k$:

$$v_k^* = (\hat{P}_k^{ij}\boldsymbol{u}^t{}_{ij}\cdot\boldsymbol{r}_k) + \nu V w. \tag{5}$$

Here V is the typical magnitude of $\boldsymbol{u}^t$ and ν is the scalar parameter whose reciprocal has the meaning of signal/noise ratio. Three values of ν (0.1, 0.3 and 0.5) were tested within

each series. In correspondence with the equation (4), HFR measurement errors in (5) were defined as $\sigma(v_k^*) = \nu V$.

To assess the impact of gaps in the spatial coverage by HFR observations, two simulated data sets were used: One with the full coverage by the radial velocity data and another without observations in the rectangular domain (right panel in Fig.1). These data sets had K=2011 and K=1699 observation points respectively.

The quality of interpolation was monitored by several parameters. Misfit between the interpolated field and the data m_d was defined as $m_d = \overline{|v_k - v_k^*|}/\overline{|v_k^*|}$, where v_k is the projection of interpolated velocity on the radar beam at the kth measurement point and overline denotes averaging over the data points. Velocity error e_v was defined as the mean absolute difference between the true $\boldsymbol{u}^t$ and interpolated $\boldsymbol{u}$ currents normalized by V:

$$e_v = \langle |\boldsymbol{u}^t - \boldsymbol{u}| \rangle / V, \tag{6}$$

where angular brackets denote averaging over the interpolation grid. Similar expressions are used to assess the interpolation qualities e_d, e_c of the divergence and vorticity fields:

$$e_d \langle |\mathrm{div}(\boldsymbol{u}^t - \boldsymbol{u})| \rangle / \langle |\mathrm{div}\boldsymbol{u}^t| \rangle; \quad e_c \langle |\mathrm{curl}(\boldsymbol{u}^t - \boldsymbol{u})| \rangle / \langle |\mathrm{curl}\boldsymbol{u}^t| \rangle \tag{7}$$

To simplify the analysis, the inverse variance W^u is set to zero in all the experiments. It is also assumed that $W^d = \gamma^{-2} W^c$, where $\gamma = 0.2$ has the meaning of the Rossby number: in most situations, the 2d vorticity field is much stronger than divergence, as the latter is driven by relatively weak vertical motions acting against gravity. Finally, since the result of interpolation depends only on the relative magnitudes of the terms in the cost function, it is convenient to characterize the 2dVar algorithm by the single non-dimensional parameter $W_*^c = \nu^2 V^2 W^c K / 4A\delta x^4 = \nu^2 K L^4 / 4A\delta x^2$ which has the meaning of the ratio between the vorticity regularization and the data misfit terms. Here $\delta x = 2$ km is the grid step and $L = 5.9$ km is the typical horizontal scale of the currents shown in Fig. 1. Since $W^d = \gamma^{-2} W^c$, the value of W_*^c entirely defines the shape of the cost function for a given field and data configuration. More details on the experimental setting can be found in [51].

Results of the experiments with three radars are illustrated in Table 1 and Figures 2 and 3. Table 1 contains errors in approximation of the true field and the data for different noise levels. It is seen that the 2dVar algorithm provides better quality of reconstruction than LI and OMA methods, although the reconstructed velocity fields look visually similar (left panels in Fig. 2). In that sense the capability of HFR measurements to capture the structure of the flows in Fig. 1 is quite remarkable. With the increase of observation noise all the algorithms loose precision, but still provide a noise-consistent fit to the data in the entire range of ν (cf. columns 2-3 and 6-7 in Table 1). The only exception is the OMA algorithm for ν=0.1 (second line in Table 1).

Reconstruction of the divergence and vorticity fields is less accurate since horizontal derivatives amplify grid-scale noise. This is especially visible in the behavior of e_d, because the divergence field was set to be five times weaker than vorticity by the design of the experiments. Nevertheless, in contrast to the OMA and LI methods, the 2dVar algorithm captures signs and positions of the major structures in the divergence field at the "practical" noise levels of 0.1 and 0.3 (upper right panel in Figures 2).

Compared to the divergence, the vorticity field is reconstructed with much higher quality: Both the amplitudes and locations of most of the structures are well reproduced even

Table 1. Dependence of the interpolated field error parameters m_d, e_v, e_c, and e_d on the reconstructed velocity field and noise level ν in the simulated HFR data. The 2dVar, OMA and LI results are shown respectively in the upper, middle and lower lines of the table cells. The smallest errors are boldfaced. Note that LI errors were computed over subdomains which did not include near-coastal regions and the gap (see Fig. 2-3). Parameters for the 2dVar and OMA interpolation schemes are shown in the right column. The 2dVar experiments with ν=0.5 were made under the divergence-free approximation ($W_*^d = 10^6$)

	no gap				gap				W_*^c
ν	m_d	e_v	e_c	e_d	m_d	e_v	e_c	e_d	L(km), κ
	0.07	**0.13**	**0.19**	**0.76**	**0.07**	**0.15**	**0.23**	**0.82**	0.2
0.1	0.26	0.31	0.38	1.52	0.28	0.39	0.50	1.70	6, 10^{-3}
	0.10	0.19	0.32	1.19	0.15	0.33	0.49	1.35	
	0.24	**0.29**	**0.37**	1.69	0.24	**0.29**	**0.41**	**1.59**	1.8
0.3	0.28	0.32	0.39	**1.66**	0.29	0.41	0.51	1.78	6, 10^{-3}
	0.22	0.30	0.42	2.07	**0.23**	0.41	0.58	1.79	
	0.41	**0.31**	**0.37**	**1.59**	0.42	**0.43**	**0.53**	**1.87**	20^*
0.5	**0.31**	0.34	0.42	1.69	**0.32**	0.44	0.56	1.93	6, 10^{-3}
	0.34	0.41	0.57	2.99	0.49	0.50	0.69	2.36	

at the noise level of ν=0.3 (cf. right panel in Fig.1 and left panels in Fig. 3). The gap in data coverage is also handled well: the overall increase in of the interpolation errors e_v, e_d and e_c in Table 1 is consistent with the fraction of the interpolation domain occupied by the gap, whereas the saddle-like structure of the vorticity field in the gap is reconstructed quantitatively by the 2dVar method.

The velocity patterns generated by the three methods (left panels in Figure 2) differ in terms of the velocity interpolation error e_v. The difference becomes more evident after taking the divergence of the fields (right panels in Figures 2 and 3): Since OMA does not impose any smoothness constraint on div$\boldsymbol{u}$, the corresponding divergence field, although being 3 times weaker than vorticity, looks rather chaotic with the formal error e_d=1.52. A similar featureless pattern is produced by LI, with the difference that divergence in near-coastal areas cannot be estimated at all due to either single-radar measurements or to beam-crossing angle limitation (nearly parallel radar beams).

Introduction of the gap in data coverage enhances the difference between the three methods (cf. columns 4-8 and 5-9 in Table 1 keeping in mind that LI errors are computed outside the gap). A probable reason for the difference between OMA and 2dVar is emergence of the spurious maxima in both vorticity and divergence fields inside the gap in the OMA case (cf. upper and middle panels in Fig. 3). In the 2dVar formulation, vorticity and divergence fields cannot have local maxima inside data-void regions, because their variation within the gap closely approaches the behavior of a harmonic function.

Comparison of the 2dVar, OMA and LI lines in Table 1 shows that OMA code tends to provide less precise fit to the data at 10% noise level without the gap (line 2 in Table 1).

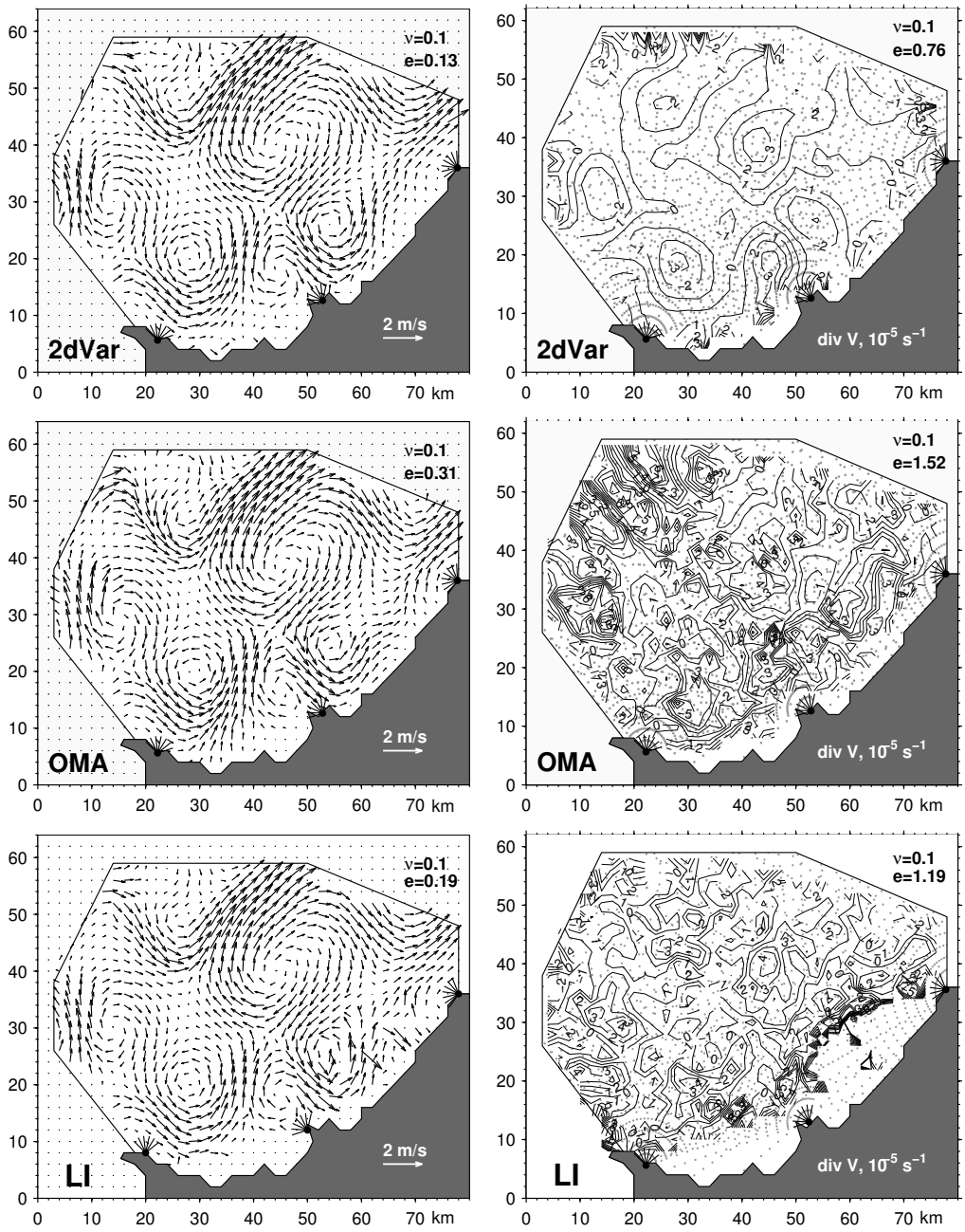

Figure 2. Comparison between the three methods of interpolation. The noise level ν and interpolation errors are shown in the upper right corners of the corresponding panels.

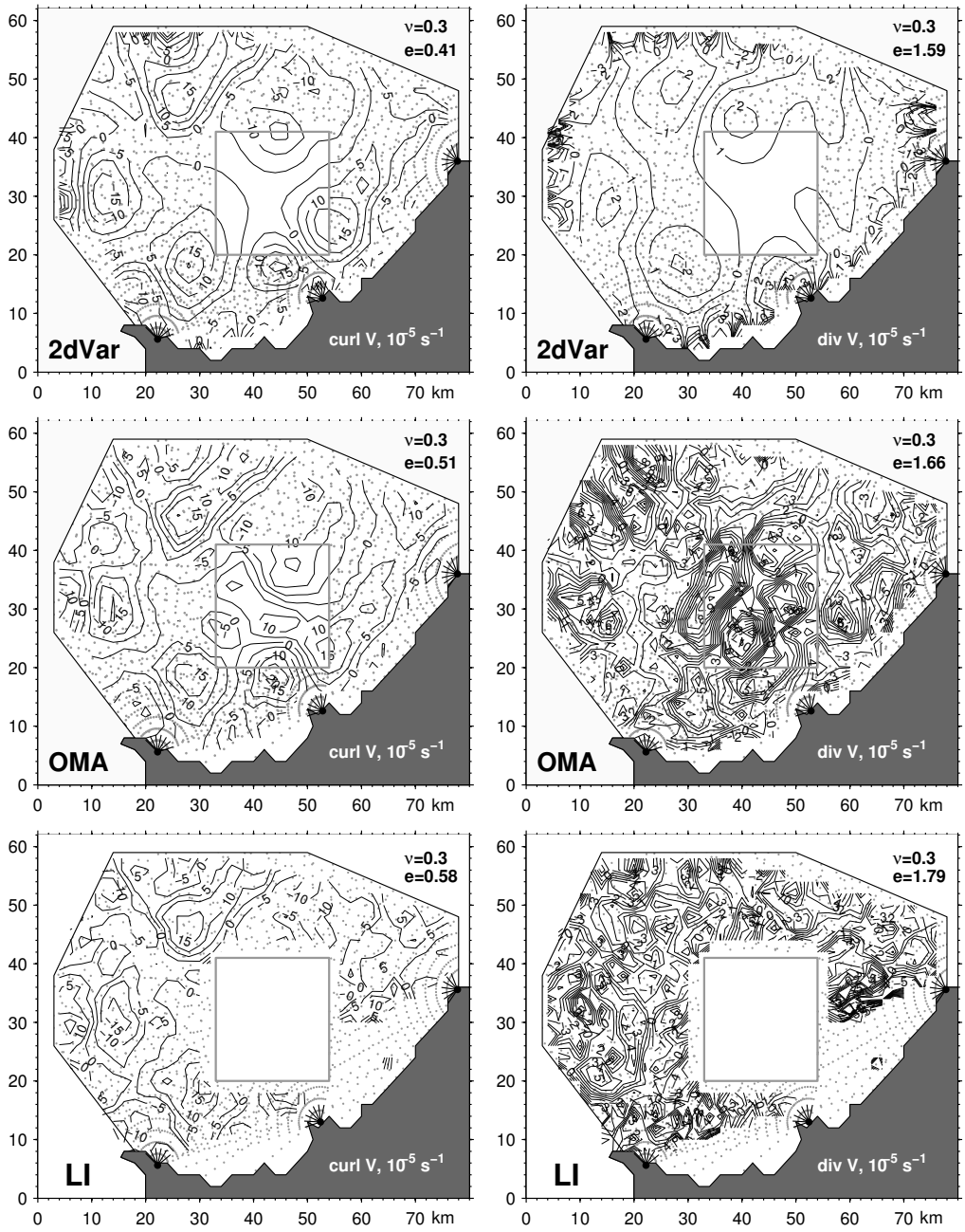

Figure 3. Comparison between the interpolations of three radars with a gap in observations. The noise level ν and interpolation errors are shown in the upper right corners of the corresponding panels.

This can be partly explained by a relatively low number of degrees of freedom (number of modes) involved. In the OMA formulation the number of modes is proportional to $(D/L)^2$ [20], where D is the horizontal size of the domain and L is the cut-off length scale. For the reported experiments, however, the optimal length scale L was close to 6 km (right column in Table 1). Such length scale corresponds to 200-230 eigenmodes, whose amplitudes were varied to fit the data in 2011 (1699 with the gap) observation points. In an attempt to achieve a better fit m_d at low noise levels, we tried to increase the number of modes by reducing L to 2-3 km, but that required an increase of regularization parameter κ, otherwise interpolation patterns appeared too noisy, possibly because of the ill-conditioning of the system matrix.

Overall, Table 1 shows that the 2dVar method performs similar to LI and better than OMA at ν=0.1 and somewhat better at ν=0.3-0.5. When the gap is present in the data (lines 1-2 and 4-5 in Table 1) 2dVar keeps a significant advantage to OMA up to ν=0.3. Both non-local methods (OMA and 2dVar) are better than LI because of their ability to estimate currents within the gap and close to the coastline.

Table 2. Same as in Table 1, but for the experiments with 2-radar configurations

radars	ν	no gap				gap				W_*^c
		m_d	e_v	e_c	e_d	m_d	e_v	e_c	e_d	L(km), κ
1,3	0.10	0.09	0.21	0.26	1.31	0.09	0.25	0.35	1.21	0.4
		0.31	0.38	0.48	1.68	0.29	0.48	0.59	2.09	6, 10^{-3}
		0.12	*0.25*	*0.42*	*1.43*	*0.17*	*0.39*	*0.56*	*1.42*	
	0.30	0.24	0.31	0.37	1.60	0.22	0.38	0.48	1.54	1
		0.33	0.42	0.51	2.07	0.31	0.51	0.65	2.37	6, 10^{-3}
		0.19	*0.39*	*0.55*	*2.35*	*0.24*	*0.61*	*0.69*	*1.82*	
1,2	0.10	0.10	0.29	0.34	1.82	0.09	0.32	0.44	1.84	0.6
		0.29	0.36	0.45	1.59	0.30	0.43	0.52	1.88	6, 10^{-3}
		0.11	*0.32*	*0.39*	*1.22*	*0.15*	*0.46*	*0.56*	*1.27*	
	0.30	0.24	0.39	0.45	2.04	0.25	0.44	0.52	2.19	0.8
		0.31	0.41	0.49	2.01	0.30	0.45	0.53	2.03	6, 10^{-3}
		0.17	*0.42*	*0.50*	*2.17*	*0.25*	*0.54*	*0.68*	*1.26*	

In practice, there are often situations when a radar stops operating due to hardware failure or some other reasons. In such case local interpolation methods often fail in a large number of gridpoints, because they require at least two velocity components for retrieving the velocity vector in a grid cell. The OMA and 2dVar algorithms are essentially non-local and therefore have an ability to interpolate the velocity field over distances exceeding the grid cell size δx.

To investigate the performance of the schemes in such situations, we switched off the rightmost (northern) and/or middle radars and examined the interpolation patterns both with and without the gap in the data. These experiments also allowed us to assess the accuracy of interpolation in the regions where data density was less or close to one observation per grid cell: After removing the northern radar such regions emerge in the upper (western) and right (northern) parts of the domain.

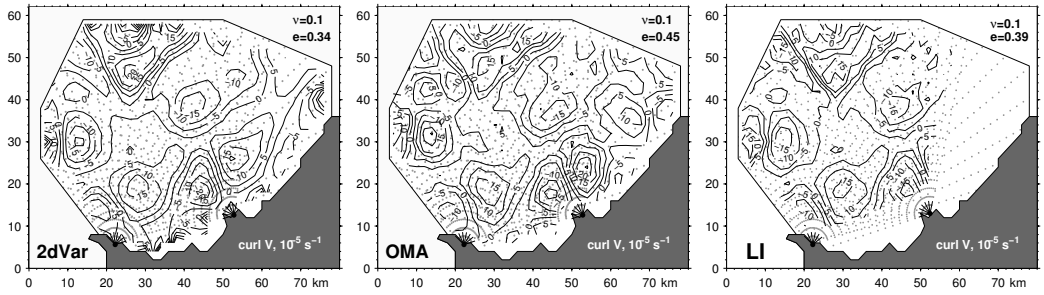

Figure 4. Comparison between the interpolations with two radars. The noise level ν and interpolation errors are shown in the upper right corners of the corresponding panels.

Figure 4 gives an indication that OMA algorithm is less accurate than 2dVar in such regions: A visual comparison of the vorticity distributions with those in Figure 1 shows that OMA errors tend to be larger when $y > 40$ km or $x >$60 km. The LI algorithm performs much worse: derivatives of the velocity field cannot be estimated not only in the region of single-radar coverage ($x >$60 km) but also near the coastline. Quantitative assessment of e_c for the three interpolation patterns in Figure 4 also shows that the regions of low data density are the major contributors to the larger value of e_c for the OMA pattern (0.45 vs 0.34 in Figure 4). The value of e_c for LI (0.39) cannot be objectively compared with these numbers because it was computed by averaging over much smaller area.

Figure 5 shows an example of interpolation with two radars and the gap in the data. The difference between 2dVar and OMA is already evident from the velocity patterns: OMA produces a spurious jet within the gap which destroys two eddies at the upper and right edges of the data-void region. 2dVar preserves these eddies and the saddle-like structure of the currents within the gap. Comparison of the vorticity fields (right panels in Figure 5) shows that OMA again produces a maximum inside the gap. The 2dVar pattern appears to be unrealistic inside the gap as well, but compared to OMA has more reasonable structure near the gap's boundary.

The overall results (Table 2) indicate that in the case of two-radar configurations non-local methods (OMA and 2dVar) have a considerable advantage over LI with 2dVar showing somewhat better performance than OMA.

2.2.2. Real Data Examples

To assess the performance of the interpolation with real data, velocity field from real HFR observations in the Bodega Bay have been reconstructed (Fig. 6). The interpolation parameters for OMA were L=5 km and κ=10^{-4} as in [20]. The 2dVar algorithm was used in divergence-free approximation ($W_*^d = 10^6$), because at the estimated noise level of ν=0.35, velocity scale of L=4.4 km and sampling discretization of 2 km, it is hard to obtain statistically confident estimates of the divergence. With 1401 observation points in use, W_*^c=0.5.

The 2dVar and OMA- generated patterns are qualitatively similar, although OMA velocity is more smooth and characterized by somewhat larger misfit with the data. The major difference between the 2dVar- and OMA-generated patterns is observed in two regions shown in Fig. 6 by gray rectangles. In the bay between the southern (left) and middle radars

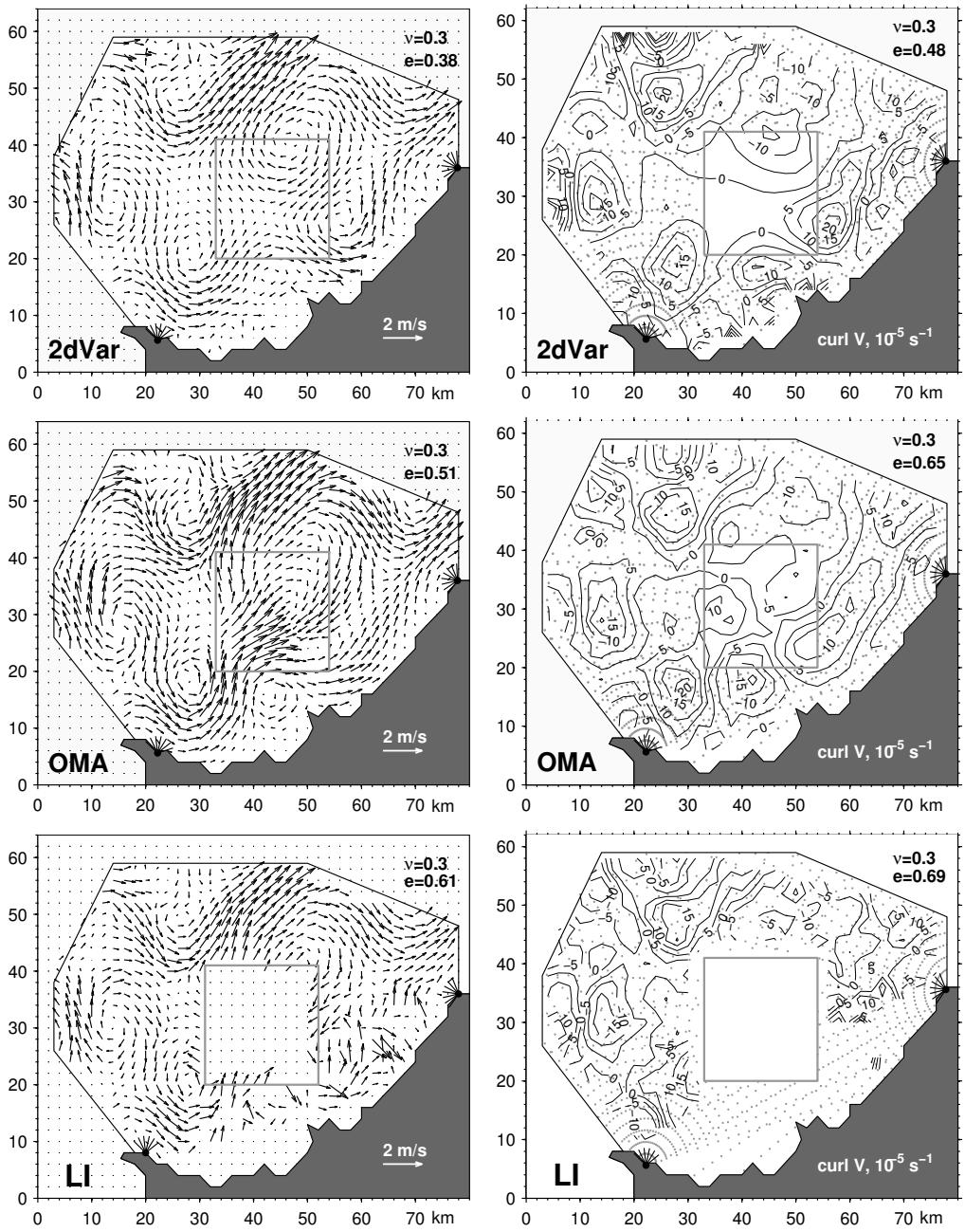

Figure 5. Comparison between the interpolations of two radars with a gap. The noise level ν and interpolation errors are shown in the upper right corners of the corresponding panels.

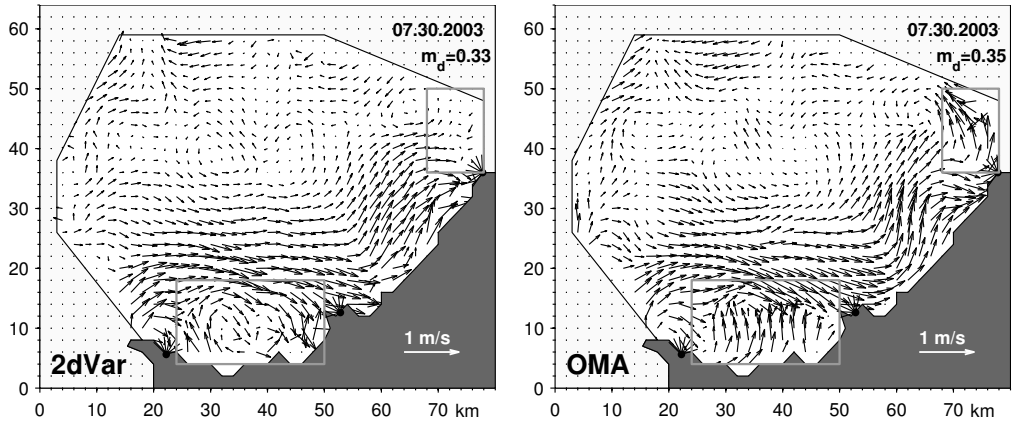

Figure 6. Velocity field in the Bodega Bay on July, 30, 2003 obtained by two interpolation methods. Misfit m_d with the radial velocity data is shown in the upper right corners.

the 2dVar pattern shows an indication of anticyclonic circulation, whereas OMA produces a broad offshore current there. The values of e_v computed by averaging over 265 observation points in that region are 0.26 for 2dVar and 0.27 for OMA respectively. The region on the right should be considered as a gap, since it contains only 4 data points near its right boundary.

The LI interpolation (not shown) appeared to have much lower quality compared to the results of non-local interpolation. This was evident not only in terms of the larger m_d=0.29, but also visually: velocity estimates do not exist in the sparsely covered right corner of the domain and are too noisy near the coast where radar beams are close to parallel.

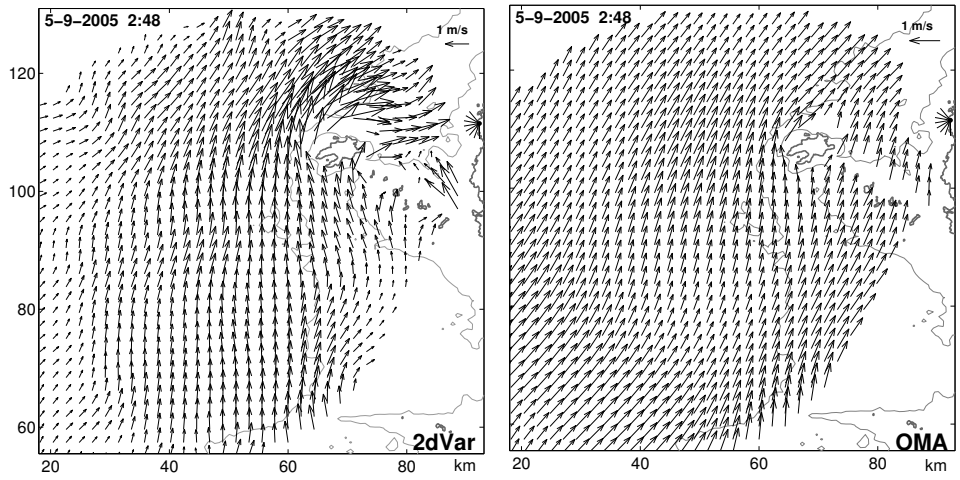

Figure 7. Surface currents in the Iroise Sea (Northern Bay of Biscay) on September 5, 2005 (02:48GMT) obtained by the 2dVar (left) and OMA methods. 50 and 100m isobaths are shown by gray contours. HFR location at Point Garchine is shown by the black dot.

Figure 7 shows a comparison of the surface current velocities obtained by the OMA

and 2dVar methods on September 5, 2005 in the Iroise Sea (northern Bay of Biscay). This area is continuously monitored by two high-frequency Wellen Radars (WERA) operating at 12.4 MHz since July 2006. The radar sites are located at the Point Garchine (Fig. 7) and Brezellec (not shown, 5 km east of the SE corner of the domain). The Beam forming (BF) method, actually used for processing the radar data in near real-time, provides radial velocities of surface current along beams with 3dB width of 9°. The along-beam resolution is 1.5 km and the maximum range is of the order of 140 km [33]. Radial velocities from two radars are interpolated routinely with LI algorithm to provide surface current maps at 20-min acquisition rate (http://www.previmer.org/observations/courants/radar_hf_iroise).

Regional currents are quite strong (up to 4 m/s), making it difficult to observe them by bottom-mounted currents meters. The flow structure is characterized by the strong horizontal shear (up to 10^{-3} s^{-1}) in the vicinity of the Ushant Islands and significant divergence induced by small-scale topographic features, controlling the velocity field.

Comparison of the velocity patterns in Fig. 7 shows better flexibility of the 2dVar algorithm in fitting the data when the local scales of variability abruptly change within the interpolation domain as it is seen on the transition from the southwestern part of the region to the region of Ushant and Molene Islands in the northeast. The 2dVar algorithm provides a significantly better resolution in that area, generating a strongly sheared flow around the Ushant Island and significantly smaller interpolation errors in this region: the root-mean-square deviations of the interpolated velocities from the observed radial velocities are respectively 0.24 and 0.39 m/s for the 2dVar and OMA-generated patterns. Specific features of regional circulation, such as the control of the flow by bathymetry, current intensification and deflection of the currents north of Ushant Island, are better reproduced by the 2dVar algorithm [44].

3. Dynamically Constrained Interpolation Techniques

Interpolation techniques discussed in the previous section are essentially two-dimensional, i.e. interpolated velocity patterns at different times are not connected neither statistically nor dynamically. In the last decades advanced interpolation methods have been developed that produce dynamically and statistically consistent estimates of the entire ocean state. These methods combine dynamical constraints from numerical models of the oceanic circulation with statistical information from observations. By using such approach it becomes possible not only to interpolate the observed data in space and time, but also infer information on unobserved variables, such as wind stress, bottom friction coefficient, vertical velocity etc. Another advantage of this approach is its ability of natural blending HFR data with other types of observations. Combining numerical models and data to make an optimal analysis is referred to as data assimilation (DA) which is now widely used in oceanography. The data assimilation methods are divided into two categories: sequential and fully four-dimensional in space-time. In this section, we give a brief overview of the existing applications of the DA techniques to HFR data.

3.1. Sequential Methods

The most widely used DA schemes optimize model solutions sequentially in time: After a model forecast is adjusted to observations, the analysis (adjusted state) is propagated forward in time by the model until new data are available. The adjustment (interpolation) is usually formulated as a weighted least squares problem with the weights defined by the error covariance matrix of the observations. In the simplest DA scheme, the error covariance does not change in time, and the problem is reduced to a sequence of OIs and model integrations of the interpolated states. The approach when both the state and its error covariance are propagated by the model is referred to as Kalman filtering (KF).

Although HFR measurements represent a very valuable data set for coastal ocean state estimation, DA of the HFR observations is only at the very beginning of the massive operational use. Comparatively simple techniques, mainly based on nudging (e.g. [50], [28]) allowed Lewis et al. [28] to optimize poorly known atmospheric forcing in the Monterey Bay, California. An approach is taken in which the HFR data act as if there were an additional layer of water overlying the ocean surface. A pseudo-shearing stress resulting from the difference between the model-predicted velocity and the Doppler radar velocity is added to that of the wind in order to force a model. However, the method had not used any knowledge of the error covariances that could improve blending of the model-predicted and observed surface currents. Furthermore, wind-forcing was corrected only at model locations that were within the HFR footprint, thus introducing a risk of unrealistic irregularities at the edges of the footprints.

Using a similar approach, Wilkin et al. [50] performed a vertical extrapolation of the HFR surface velocities. In the experiments, a statistical projection scheme based on correlations between the HFR and the moored Acoustic Doppler Current Profiler data was used. The experiments showed that HDR data provides an invaluable source of information for coastal ocean DA forecast systems and that even a simple statistically based vertical extrapolation significantly improves the skill in estimating subsurface velocities in New Jerseys shelf region.

In a number of recent studies [9, 36, 37, 5] sequential DA schemes were used assimilate the surface currents with covariance estimates based on the ensembles. Oke et al. [36] performed an assimilation of low-pass filtered surface velocity observations from coastal HFR arrays into a primitive equation coastal ocean model. The error covariance model was obtained from the ensemble of model simulations and involved correlations between the surface velocity and the subsurface fields of temperature, salinity and velocity. Using these inhomogeneous error covariances among the model variables, the 3d model corrections based on the surface-only HFR data were derived and successfully used in the DA scheme. The correlation between subsurface current measurements and subsurface currents obtained from model was improved two times (from 0.42 to 0.78), when radar data were assimilated, thus demonstrating the effectiveness of such DA approach.

In a similar manner, a 3d covariance matrix for the Princeton Ocean model model has been constructed by Breivik and Saeťra [9] who used a statistically representative reference model run. The matrix has been kept fixed throughout the assimilation period. The ensemble KF based optimal interpolation of HFR velocities recorded off the Norway coast, has been used to provide dynamically balanced current fields generated by a system of nested

ocean models in near-real time. The system was found to yield good analyses, whereas the short range forecasts were significantly improved by assimilating HFR data.

Another sequential DA scheme based on 3dVar approach was recently developed by Li et al. [29] for operational assimilation of multiple data sets collected in Southern California into the Regional Ocean Modeling System (ROMS). The model is able to assimilate surface current observations from HF radar network. Inhomogeneous and anisotropic error covariances have been constructed by blending ensemble runs with heuristic covariance functions, and a variety of observational data collected during the Autonomous Ocean Sampling Network (AOSN) experiment (Monterey Bay, August 2003) was assimilated. The model velocities were compared with HFR and mooring observations, demonstrating a reasonable accuracy and indicating that the system is capable of reproducing complex flows associated with upwelling and relaxation, as well as the rapid transitions between them.

The approach of Lewis et al. [28] was recently revisited by Barth et al [4, 5, 6] who assumed that the larger part of the model error in surface currents might be attributed to errors in surface winds. Using the model error covariance estimated from an ensemble of model runs driven by different wind-forcing, Barthe et al. [5] assimilated radial velocities recorded by the HFRs on Florida shelf. The assimilation skill was assessed by comparing the model results with independent ADCP measurements. As expected, the largest improvement was observed at the surface but the model skill relative to the free model run was significantly improved also at depth. Later on, sequential assimilation of HFR data performed by Barth et al., [6] improved the wind forcing instead of directly modifying the model state vector. The authors used an ensemble-based assimilation scheme and 3d coastal circulation model applied this time to the German Bight region.

Sequential methods described above use a prior estimate of the forecast error covariance matrix that can be difficult to obtain in practice. Although these methods produce dynamically and statistically consistent estimates of the ocean state and they are capable of improving the model forecast skills, they do not produce a completely dynamically consistent interpolation of the data in both space and time. This task can be accomplished by the 4dVar analysis and Kalman smoothing.

3.2. 4-Dimensional Analyses

Devenon [12] was among the first who attempted to perform the dynamically constrained interpolation of HFR data using a variational approach and an adjoint-based assimilation scheme. A simple numerical model (two-dimensional linearized spectral tidal model) was used to smooth and interpolate HFR observations in a limited size coastal area (the Seine river Bay). The method constrains circulation to simultaneously agree with observations and with the hydrodynamic laws governing tidal circulation in the Bay. Moreover, the HFR data have been used to identify boundary conditions for the principal M2 tidal constituent, and the bottom friction coefficient.

Similar approach was used by Sentchev and Yaremchuk in the Strait of Dover [41] and English Channel [43]. The open boundary conditions of the finite-element spectral tidal model [27] were optimized to fit the HFR surface velocities and coastal tidal gauge data. The result of interpolation was used for mapping of the residual transport through the Channel, tidal dissipation, and for estimation of the energy flux. Analysis of the residual

flow stream function revealed a number of permanent eddies associated with peculiarities of the coastline shape and inhomogeneities of the bottom topography. Extensive error analysis of the results was conducted via an explicit inversion of the Hessian matrix, associated with the DA scheme. Error charts for the sea surface elevation demonstrated the model's ability to fit the data within the error bars and exposed coastal areas requiring better coverage by observations.

Another study of tidal currents was made by Kurapov et al. [24, 25] who retrieved harmonic tidal constituents from the HFR observations off the Oregon coast. The 3d baroclinic spectral tidal model was coupled with the representer-based 4dVar method [8]. Computations with synthetic data (tidal velocity ellipses) showed that HFR observations at the surface can also be used to map tidal flow at depth. For the M2 tidal constituent, information from the surface was projected in space-time along the wave characteristics, thus providing a uniquely detailed picture of the temporal and spatial variability of internal tide on the central Oregon shelf.

In a more general study, Hoteit et al. [19] combined a high resolution configuration of the Massachusetts Institute of Technology general circulation model and its adjoint to obtain a dynamically consistent interpolation pattern that matches HFR data collected off the San Diego coast in California. The DA scheme adjusted initial conditions, boundary conditions, and atmospheric forcing fields to match a model solution to observations. The dynamically constrained interpolation experiments have shown that the model solutions can be tuned to match HFR observations within the error bars over the period of 10 days, largely through the adjustment of the wind stress controls. Similar results were obtained in [38, 6] who identified wind uncertainties as the major source of errors in coastal models. Thus, continuous assimilation of HFR data provides an efficient and dynamically consistent tool to correct these errors and significantly increases the 24-hour forecast skill in the modeling of sea surface currents.

4. Reconstruction of the Missing Data

As it has been already mentioned, the unique feature of HFR observations is their nearly continuous temporal and spatial coverage. However, the back-scattered HFR signals are subject to distortions of artificial and natural origin which cause numerous gaps in spatial coverage. These gaps may strongly degrade performance of the interpolation algorithms.

The impact of the missing radial velocity data can be diminished by taking into account temporal statistics of the HFR observations which allow to obtain spatial covariances with a reasonable degree of accuracy. Therefore, an interpolation algorithm in the space of radial velocities can be thought out which fills the gaps using a truncated EOF decomposition of the data covariance matrix. This technique is widely used in processing the SST imagery, and can also be readily applied to HFR observations [53]. In addition, spatial correlations between the radial velocities can be used to estimate observational noise, assess its variance, and, therefore quantify the cost function weights of the 2dVar interpolation algorithm (4).

4.1. The Method

The spectral decomposition provides the following representation of the covariance matrix:

$$\boldsymbol{C} = \boldsymbol{U}\Lambda\boldsymbol{U}^{\mathsf{T}}, \tag{8}$$

where $\boldsymbol{U}$ is a rectangular matrix whose columns are the eigenvectors $\boldsymbol{e}^k$ (empirical orthogonal functions, EOFs) of $\boldsymbol{C}$ corresponding to the eigenvalues λ_k, and $\Lambda = \mathrm{diag}\{\lambda_k\}$. The eigenvalues quantify time variation of the spatial patterns in the radial velocity distributions described by the corresponding EOFs.

Representation (8) can be employed to estimate the noise level using the cross-validation (CV) technique (e.g., [7]). The technique provides a certain number of EOFs (modes) K_r that are well-resolved by the HFR observations. The rest of the modes $\boldsymbol{e}^k$, $k > K_r$ are attributed to noise, whose spatial variability cannot be determined with statistical confidence from the data. Technically, K_r is computed as the number of modes which minimize the interpolation error at the randomly chosen set ω_c of CV points. These points are temporarily removed from observations and constitute a small portion of the data set in order to minimize their impact on the result of covariance estimate.

To fill a gap containing points $\boldsymbol{x}_i$ in a subdomain $\omega \subset \Omega$, the radial velocities $v(\boldsymbol{x}_i)$ observed outside the gap ($\boldsymbol{x}_i \in \Omega \setminus \omega$) are expanded in K_r "resolved" eigenfunctions $\boldsymbol{e}^k$ of $\boldsymbol{C}$:

$$\text{find } \alpha_k : \sum_{\boldsymbol{x}_i \in \Omega\setminus\omega} \left[\boldsymbol{v}(\boldsymbol{x}_i) - \sum_{k=1}^{K_r} \xi_k \boldsymbol{e}^k(\mathbf{x}_i) \right]^2 \to \min_{\xi_k} \tag{9}$$

and the expansion coefficients ξ_k are used to obtain radial velocities within the gap:

$$\boldsymbol{v}(\boldsymbol{x}_i \in \omega) = \sum_{k=1}^{K_r} \xi_k \boldsymbol{e}^k(\boldsymbol{x}_i \in \omega) \tag{10}$$

After this, the EOF expansion is iteratively improved: a set of EOFs $\{\boldsymbol{e}^k_{(m)}\}$ on the mth iteration is computed using the covariance estimate $\boldsymbol{C}_{(m)}$ emerging from the data set whose gaps are already filled with the help of the previous EOFs $\{\boldsymbol{e}^k_{(m-1)}\}$, then these new EOFs $\{\boldsymbol{e}^k_{(m)}\}$ are employed to fill the gaps again. The process terminates when the relative reduction of the mean interpolation error

$$\varepsilon^2(K_r) = \sum_{\boldsymbol{x}_i \in \omega_c} \left[\boldsymbol{v}_c(\mathbf{x}_i) - \sum_{k=1}^{K_r} \xi_{(m)k} \boldsymbol{e}^k_{(m)}(\boldsymbol{x}_i) \right]^2 \tag{11}$$

computed over the CV set ω_c becomes smaller than the machine precision. Computations described by (9-11) are conducted for several values of K_r to find the optimal one that minimizes ε^2.

With the optimal cutoff number of modes K_r, the covariance matrix $\boldsymbol{C}$ can be decomposed into the well-resolved $\boldsymbol{C}_r$ and unresolved (noisy) $\boldsymbol{C}_n$ constituents:

$$\boldsymbol{C} = \boldsymbol{C}_r + \boldsymbol{C}_n \equiv \boldsymbol{U}_r\Lambda_r\boldsymbol{U}_r^{\mathsf{T}} + \boldsymbol{U}_n\Lambda_n\boldsymbol{U}_n^{\mathsf{T}} \tag{12}$$

where $\boldsymbol{U}_r$ is the $K_r \times K$ matrix, whose columns are the first (well-resolved) eigenvectors, $\Lambda_r = \mathrm{diag}\{\lambda_k\}, k = 1,...,K_r$; the eigenvectors in the columns of the $(K-K_r)\times K$ matrix $\boldsymbol{U}_n$ are attributed to noise, and $\Lambda_n = \mathrm{diag}\{\lambda_k\},\ \ k = K_r+1,\ldots,K$.

The noise level ν is estimated as

$$\nu = \left[\frac{\mathrm{Tr}\Lambda_n}{\mathrm{Tr}\Lambda}\right]^{\frac{1}{2}} \equiv \left[\sum_{i=K_r+1}^{K}\lambda_i \Big/ \sum_{i=1}^{K}\lambda_i\right]^{\frac{1}{2}} \tag{13}$$

whereas observation error variances $\sigma_k^2,\ k = 1,...,K$ (Eq. (4)) are represented by the diagonal elements of the matrix $\boldsymbol{C}_n = \boldsymbol{U}_n\Lambda_n\boldsymbol{U}_n^{\mathsf{T}}$. The diagonal elements of $\boldsymbol{C}$ can also be utilized to estimate the variances σ_u^2, σ_c^2 and σ_d^2 of the respective fields $\Delta\mathbf{v}$, $\Delta\mathrm{curl}\mathbf{v}$ and $\Delta\mathrm{div}\mathbf{v}$ which enter the equation (4) in the form of the inverse variances W^u, W^c and W^d.

In the next section, the benefits of the GF technique are assessed in a series of experiments with simulated and real data.

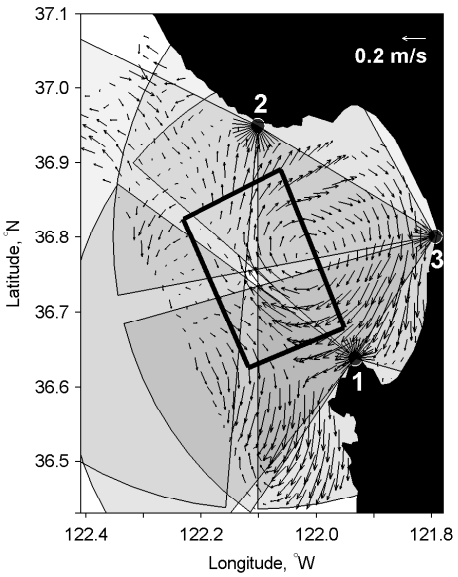

Figure 8. Setting of the gap simulation experiments: Gray shading shows data acquisition areas of the radars in the presence of a simulated ship (case *b*) moving across the Monterrey Bay. Area within the rectangle shows the boundary of the data-free region in case *c*. Numbers enumerate radars switched off in case *d*.

4.2. Testing

4.2.1. Experiments with Simulated Data

Experiments with simulated data were configured to mimic real observations conducted in the Monterrey Bay in summer of 2003 [48]: The "true" currents $\boldsymbol{u}^t$ were extracted from the 12.5-day run of the NCOM model [3] forced by COAMPS [18] winds. Surface currents were sampled every hour along the beams of three radars which probed the

radial components v_k^* of the model surface velocity at 386, 407 and 349 points respectively. Therefore the dimension of the data space was K=1142. The total number of the grid points where velocity vectors were reconstructed was M=560, so the number of unknowns $2M$=1120 was approximately equal to the number of observations. Overall there are $N = Kn = 1142 \cdot 301 = 343,742$ observation points, where n is the number of hourly time steps in the 12.5 day time window. Observations were modeled by eq. (5)

Three noise level values ν (0, 0.1, and 0.3) were tested within each of six major series of experiments. Each series was characterized by specific structure of the artificial gaps introduced into the simulated data set to assess the benefits of the GF technique. These simulated data sets were the following:

0) without the gaps

a) with 1-point gaps randomly distributed along the beams (data loss γ=13.5%)

b) with gaps, generated by obstacles, moving across the domain (Fig. 8): Each obstacle (ship) spoils data along three beams, whose intersection point coincides with the ship's position. Back-and -forth motion of three ships, which effectively removed 6.9% of the data points from observations was simulated.

c) with the gap created by discarding all observation points in the rectangular region (Fig. 8) for 1 day. This gap removed 28% of the data on August 10-11 and approximately γ=2% of the data overall.

d) with gaps generated by switching off for 12 hours radars 2,3 on August 4, radar 1 on August 8 and radars 1,3 on August 12 (Figure 8, γ=6.3%).

e) with all the above mentioned gaps superimposed (γ=28.2%)

The quality of interpolation was monitored by the same three parameters e_u, e_c and e_d as described by eq. (6-7), The CV set ω_c was specified by randomly removing 10-13 points on each time layer with the total number of CV points N_{cv}=3,490 (approximately 1%).

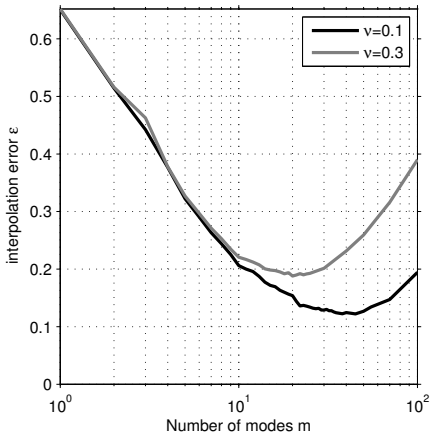

Figure 9. Interpolation error ε as a function of the number of modes m.

The cutoff number K_r was determined for the noise levels (ν=0, 0.1 and 0.3) by minimizing the interpolation error (11), and was found to be independent on random variations in the space-time structure of the CV set. Figure 9 shows calculations of K_r for the experiments with ν=0.1 and 0.3: for observations specified by eq. (5) the S/N separation number

is 38 for ν=0.1 and 20 for ν=0.3. The corresponding estimates of the noise level (Eq. (13)) are 0.093 and 0.29 in very good agreement with the true values. For the case of perfect observations ($\nu = 0$) K_r appeared to be close to K as the dependence (11) $\varepsilon(K_r)$ flattened out at large K_r and did not show any distinct minimum.

Table 3 shows the improvement in performance of the 2dVar algorithm when the preliminary GF is applied.

Table 3. Dependence of the interpolated field parameters e_v, e_c, and e_d on the structure of the gaps in HFR observations for $\nu = 0.3$. The results of standard 2dVar (without GF) and 2dVar with the gaps filled are shown respectively in the left and right columns of the table cells

case	γ	e_v		e_d		e_c	
0	0.0%	——	0.251	——	0.652	——	0.537
a	13.5%	0.260	0.252	0.665	0.659	0.551	0.542
b	6.9%	0.256	0.251	0.662	0.654	0.545	0.540
c	2.0%	0.254	0.251	0.660	0.655	0.545	0.539
d	6.3%	0.280	0.258	0.677	0.661	0.564	0.542
abcd	27.9%	0.311	0.274	0.703	0.679	0.589	0.558

In the case *a* (randomly distributed 1-point gaps) the improvement is significantly lower than the percentage of data loss (13.5%), primarily because filling random 1-point gaps affects information content on the grid scale which is poorly resolved anyway. Besides, data absence is largely compensated by observations in the points located in the immediate vicinity of the 1-point gaps at distances often smaller than the grid step. These neighboring points compensate missing data and provide the 2dVar interpolation with enough information on the larger-scale variability. Also note that the surface velocity field is recovered in most cases with a better accuracy e_v than the noise level $\nu = 0.3$.

Moving ships (case *b*) spoil 6.9% of the entire set of 343,742 data points. Relative improvement of the 2dVar interpolation (line 3 in Table 3) is somewhat smaller than for the case of completely random gaps: Velocity field is better by 1.1% whereas vorticity and divergence fields show 0.9 and 1.0% improvements respectively. Nevertheless, the improvement appears to be pretty robust with respect to this type of gaps as well.

Much more difficulties emerge when a gap occupies a significant portion of the interpolation domain, as in case (*c*) (Fig. 8). To better illustrate the benefits of the GF technique, we placed the gap at the location of an eddy-like structure seen in the mouth of the Monterrey Bay around the 10th of August, 2003 (Fig. 10, left panel). This eddy is not reproduced by the 2dVar technique alone (Fig. 10, right panel), simply because there is no information on the eddy in the velocity field, surrounding the gap. On the contrary, if GF is used prior to 2dVar, a certain portion of this eddy emerges from the EOF statistics, increasing the skill of the 2dVar algorithm (Fig. 10, middle panel).

Table 3 does not give full impression of the improvement, because error data are averaged over the whole observation period (12.5 days), whereas the data sets in case (c) differ only on the 10–11th of August. If averaging is performed over the time period containing

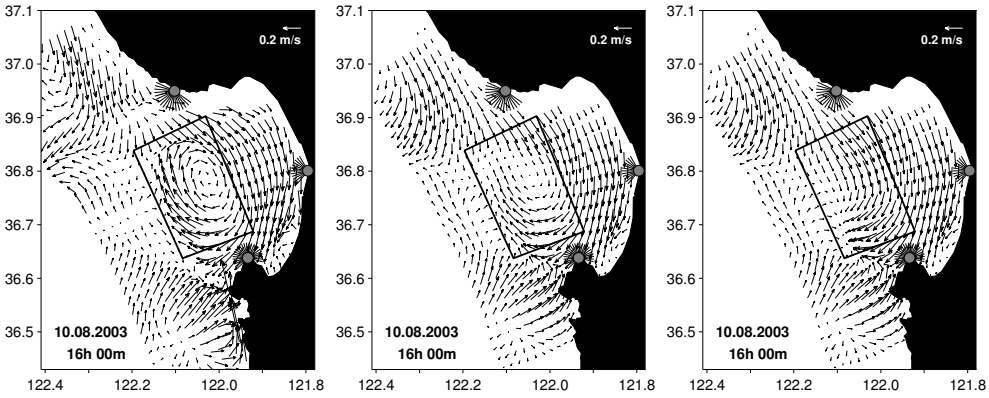

Figure 10. The "true" velocity field (left panel) and velocity fields reconstructed by 2dVar with preliminary filling the rectangular gap (middle panel) and without (right panel).

the gap (from 12PST 10.08.2003 to 12PST 11.08.2003) then the advantage is obvious: e_v is reduced from 0.49 to 0.32 (33% reduction). Similar error reductions are also observed for the vorticity and divergence fields (28 and 37% respectively).

A common reason for low data return of a HFR system is malfunction of one or more radars. This kind of situation was simulated by switching off both northern radars for half a day on the 4th of August, southern radar on the 8th and two southern radars on the 12th. The strongest reduction of the interpolation errors occurred on the 12th of August, when the reconstructed (true) currents were generally perpendicular to the beams of the only operating radar. In that case the velocity error e_v reduced 64% (from 0.84 to 0.34) with 66% of the missing data being filled. Interpolated velocity distributions show that 2dVar tends to align velocities along the beams of the only working radar, producing rather unrealistic patterns. After filling of the missing data from the southern radars, the skill of the 2dVar algorithm was significantly improved.

Finally, all the gaps were combined together to obtain a "realistic" HFR record, characterized by 72% of the data return. Figure 11 gives an overall comparison between the methods in terms of e_v, e_d and e_c. It is obvious that EOF-based GF of the radial data is particularly advantageous during the severe data loss events caused by either malfunction of a radar (8.8) or two (4.8, 12.8); or by data loss in a region, whose size is considerably larger than the grid step (11.8).

Beyond these periods, when only 1-point and ship-generated gaps are present, preliminary GF still has some (1-3%) advantage over the stand-alone 2dVar in terms of e_v, e_d and e_c (see Table 3 and Fig. 11).

It is also noteworthy that the GF technique allows to retrieve the sea surface state with the accuracy of e_v=0.27, that is better than the noise level ν=0.3 (Fig. 11) even in the case of 28% loss of observations. The conventional 2dVar technique (e_v=0.31, blue line in Fig. 11) demonstrates somewhat lower skill, primarily because of much poorer performance during the heavy data loss periods.

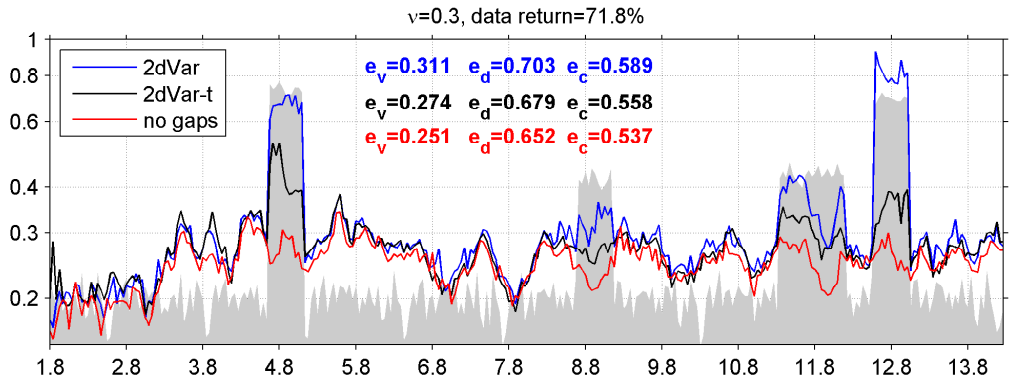

Figure 11. Velocity interpolation error e_v for the "perfect" data set (without gaps, red line), for the gappy data with (black) and without (blue) preliminary GF. Shaded area denotes the part of data occupied by the gaps. Particularly severe losses of data are observed during simulated radar malfunctions (4, 8 and 12 of August) and on August 11th, when "observations" were removed from a large region shown in Fig. 8.

4.2.2. HFR Observations in the Eastern English Channel and Iroise Sea

To test the algorithm with real data, the GF algorithm was applied to HFR observations obtained off the Opal coast of France [42] and in the Iroise Sea (northern Bay of Biscay).

The Opal coast experiment was conducted in May-June 2003 with two HFRs deployed on the Cape Gris Nez (CGN) and Wimereux (WMX, Figure 12). The entire 35-day record from 0.00 GMT 01.05.2003 to 23.40 GMT 04.06.2003 was used for testing. Surface currents were sampled every 20 minutes at 10° azimuthal resolution defined by the beam width. The radial velocity data were available along the beams at 1.8 km resolution. Grid cells with less than 75% data returns were excluded from consideration, constraining the interpolation domain to the ranges less than 20 km [43] and the total number of quality data points to K=203. Overall, the analyzed records were characterized by 87% of data return. Approximately 10% of the missing radial velocities were due to data acquisition problems at the Wimereux radar on May 3 (3 hour gap) and May 21-22 (21 hours). The instrumental accuracy of the measurements was 5 cm/s and the typical magnitude of the observed radial velocities was V_r =0.35 m/s.

A set of CV points ω_c was generated by randomly removing 8-12 radial velocities from the data every 20 minutes. In total, 24,097 (4.7%) observations were removed.

The quality of interpolation was estimated as the mean absolute difference between the values of the interpolated velocity at the CV points and the radial velocities measured at these points:

$$e_v^* = \langle | v_k - \hat{P}_k \mathbf{v} \cdot \mathbf{r}_k | \rangle$$

Here index k enumerates the CV points and angular brackets denote averaging over ω_c. The total number of gaps in observations (including the CV points) was 92,156 (18%).

Similar to twin-data experiments, the noise level was determined by minimizing the GF error (11). Dependencies of the normalized interpolation errors ε and e_v^* on the number of modes were similar to those shown in Fig. 9 and demonstrated distinct minima at K_r =

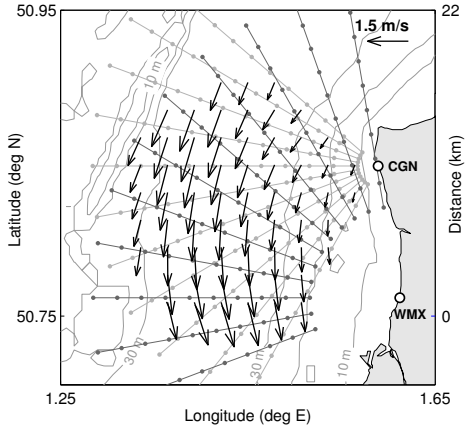

Figure 12. Surface velocity at 14.20GMT on May 21 2003 in the ERMANO study area. Contours show the bathymetry in meters. Gray dots indicate locations of the surface velocity measurements by two radars (shown by circles).

$33-35$. The value $K_r = 33$ was selected as the noise cutoff number. The corresponding observational noise level computed through eq. (13) was close to 0.15, or 5.1 cm/s, in a good correspondence with the above estimate of the instrumental errors.

Overall, the GF technique enabled to reduce the time averaged relative interpolation error e_v^*/V_r to 0.16 (5.5 cm/s), a value very close to the observational noise level. On the contrary, the mean value of e_v^* without preliminary gap filling appeared to be more than two times higher (0.35) indicating a significant benefit of combining 2dVar interpolation with the GF analysis.

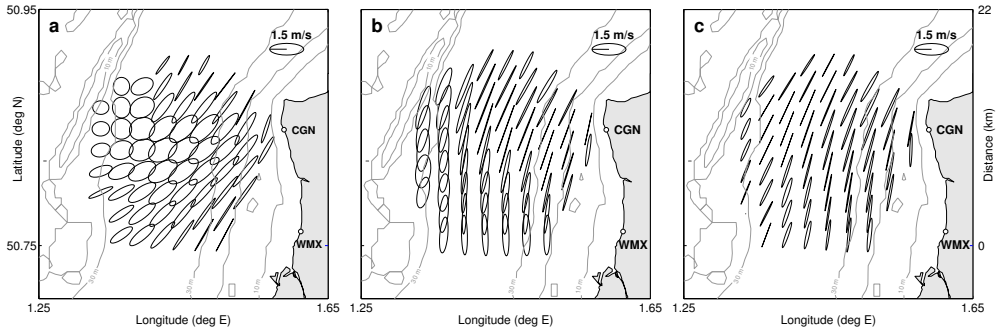

Figure 13. Tidal ellipses computed from the PCA of the surface velocities obtained by the standard 2dVar method (a); and by the 2dVar method with GF technique (b,c). The 24-hour PCA averaging is performed over the period of one operating radar (starting 12.40GMT 21.05) for (a) and (b) and over two 24-hour intervals preceding the gap (starting 12.40 20.05) and following immediately after (starting 12.00 22.05) for (c). Every second ellipse is shown.

The advantage of the GF technique is most vividly seen during the periods when the WMX radar was not working. As an example, Fig. 12 demonstrates a velocity snapshot

within the second (21-hour) gap. As it was proved by comparison with the velocity patterns obtained for the identical tidal phase on May 20 and 23, the reconstructed velocities represent well the realistic current field. Fig. 13 shows tidal ellipses from Principal Component Analysis (PCA) of the interpolated currents over the 24-hour period from 12:00 GMT 05.21.2003 to 12:00 GMT 05.22.2003. In this time interval, the WMX radar was not operating for nearly 21 hours (from 12:40 GMT 21.05 to 8:20 GMT 22.05). The pattern in Figure 13a (obtained without preliminary GF) appears to be completely unrealistic as the major axes of the ellipses tend to align along the beam directions of the only operating radar at Cape Gris Nez. Figure 13b is apparently more close to reality since the spatial distribution of the ellipses is much more similar to the ones obtained from PCA analyses of two 24-hour periods: one immediately before and another one immediately after the gap (Fig. 13c). During these two periods both radars were in full operation with the average data return of approximately 92

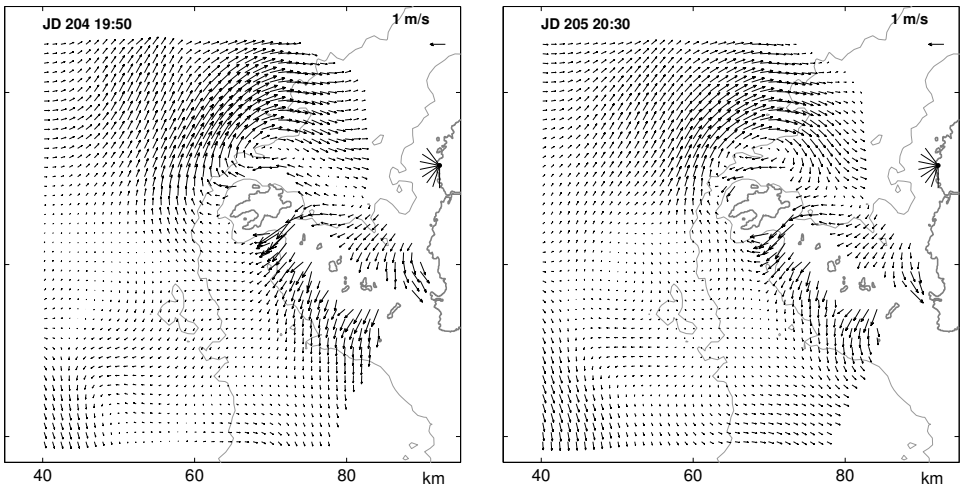

Figure 14. Right: surface currents in the Iroise Sea (West Brittany) obtained from radial velocities measured by single radar (not shown, located 5 km east of SE corner of the domain) on July, 23, 2008; velocities of the northern radar were interpolated using the GF technique. Left: surface currents in the same area measured by both radars two tidal periods earlier (July 22, 2008). 50 and 100 m isobaths are shown by gray contours. Northern radar at Point Garchine is shown by black dot.

In a similar way, the GF technique was applied for processing of the HFR data in the Iroise Sea (section 2.2.2) acquired July 21 to September 15, 2008. During that period, the radial velocity records had two major gaps. The first 4-hour gap was caused by emission interruption of the northern radar on July 23 between 18:00 and 22:00GMT. The second, 19-hour long, was caused by interruption of the southern (Point Brezellec) radar on July 28-29. Tidal currents were substantially stronger on July 23 than on July 28 thus inducing a rotational character of local circulation around the Ushant Island and Sein Archipelago.

Figure 14 shows snapshots of surface currents separated by exactly two tidal cycles (on July 23 and July 22, 2008). The circulation pattern in Fig. 14a has been obtained from one-radar data using the GF algorithm in conjunction with 2dVar interpolation. This

allowed reconstruction of the surface currents at a level of details that was not previously available. An anti-cyclonic eddy north of the Ushant Island, generated at the end of flood, is fully resolved, general pattern of circulation during the current reversal is well reproduced, as well as the current intensification in the Fromveur Strait. All these features of local circulation can be also found on the map derived from radial velocities recorded by both radars one day before (Fig. 14b). Discrepancy between the radial velocities observed by the southern radar and the interpolated velocities projected on radar beams remains below 30%. Further assessment of the GF algorithm is currently underway in the regions with low tides, (Gulf of Lyons in the Mediterranean Sea [15]).

5. Summary

Monitoring surface currents in coastal areas with HFRs is a rapidly developing application of the radar technology. Of particular importance is the HFRs' capability to observe circulation up to 150-200 km offshore with spatial and temporal resolutions sufficient for accurate tracking and prediction of floating particle trajectories, be it oil spills or rafts with people waiting to be rescued.

In this chapter we have reviewed the latest developments in the algorithms for retrieving the surface velocity field from the radial velocities. The radials are derived by processing backscattered HFR signals, a technique equally important for increasing spatial resolution and overall quality of the surface velocity field (see, for example, [31] and references therein).

In Section 2, a numerical algorithm based on minimization of a quadratic cost function in the space of all possible configurations of the velocity field was presented. Performance of the method is compared with the LI and OMA algorithms. It is shown that the 2dVar approach is robust and capable to provide a statistically consistent fit to the data in the wide range of signal/noise ratios. The comparison demonstrated similar (to LI) or better (than OMA) performance of the 2dVar technique under relatively high signal/noise ratios, especially when a 80%–90% fit to the velocity field containing strong localized features is required. At more realistic (less than 3-4) signal/noise ratios the OMA and 2dVar have similar skill and outperform LI because of their better treatment of the coastal regions where beam directions are close to parallel.

Comparison of the algorithms has also shown that the variational approach gives more flexibility in fitting the data, since the number of modes in use is close to the number of points on the interpolation grid. 2dVar method is also flexible in the choice of regularization, because the desired smoothness and its spatial variation can be directly controlled by a simple modification of the cost function weights. The method also appears to be more accurate than LI and OMA in the regions with sparse data coverage, and within the large gaps in observations.

The 2dVar algorithm is regularized by enforcing smoothness in the interpolated patterns of divergence and vorticity. This formulation attempts to retrieve spatial distribution of these quantities because they are extremely important for successful tracking of surface contaminants and other applications (search and rescue, route optimization).

Section 3 provides an overview of more sophisticated interpolation techniques, which synthesize HFR data with other observations and dynamical information provided by the

numerical models of oceanic circulation. This type of interpolation has been under extensive development in the last decade, but HFR data were rarely considered even in regional applications possibly because of their limited availability compared, for example, to satellite observations. Nevertheless, it has been shown that using HFR data greatly improves the forecast skill of the DA systems, especially when increased predictability of the surface currents is required.

An open question in HFR data assimilation is whether the radial velocities require preprocessing or should be assimilated directly into the numerical models. We assume that in many cases preliminary preprocessing could be beneficial. In particular, kinematically constrained interpolation of the HFR radials on the model velocity grid may inhibit spurious fast waves arising in the case of strongly intermittent data availability which is often observed in the practice of HFR measurements.

In Section 4 we demonstrated the benefits of more sophisticated preprocessing, which combines the EOF analysis with the 2dVar interpolation technique. This approach is able to successfully process occasional single-radar coverage events and improve the overall quality of monitoring of sea surface currents by the HF radars. The EOF analysis of the radial velocities provides a) statistically rigorous estimation of the weights for the 2dVar algorithm, and b) a set of spatial patterns (EOFs) capable to fill large gaps in the data caused by radar malfunctions. The approach takes the advantage of the frequent time sampling by the HFRs and employs observation history to estimate the leading modes of variability of the radial velocities. Numerical experiments with simulated and real data have shown that preliminary gap-filling is extremely beneficial during occasional periods of heavy data loss associated with radar malfunctioning: With the proposed technique, the 2dVar interpolation errors during these periods are typically reduced 1.5 - 2 times providing much more realistic velocity distributions (Fig. 11, 14).

Overall, an advanced interpolation method can be summarized as a four-step procedure: EOF analysis of the radial velocities; estimation of the noise and the 2dVar cost function weights; filling large gaps in observations, and finally, retrieving of the velocity vectors from the filled data set. This type of interpolation eliminates disruptions in HFR observations of surface currents caused by environmental factors and by discontinuities in HFR operation.

Further development of the preprocessing/interpolation techniques for the HFR radial velocities and their assimilation into the numerical models is a necessary prerequisite of continuous improvement in monitoring near-coastal circulation which is extremely important in practical applications and may help to solve many environmental problems caused by human activity.

References

[1] Alvera-Azcarate A., A. Barth, M. Rixen and J.M. Beckers, 2005: Reconstruction of incomplete oceanographic data sets using empirical orthogonal functions: application to the Adriatic Sea surface temperature, *Ocean Modelling*, 9, 325-346.

[2] Alvera-Azcarate, A., A. Barth, J.-M. Beckers, and R. H. Weisber, 2007: Multivariate reconstruction of missing data in sea surface temperature, chlorophyll, and wind satellite fields, *J. Geophys. Res.*, 112, C03008, doi:10.1029/2006JC003660.

[3] Barron, C.N., A.B. Kara, H.E. Hurlburt, C. Rowley, and L.F. Smedstad (2004), Sea surface height predictions from the global Navy Coastal Ocean Model (NCOM) during 1998–2001, *J. Atmos. Oceanic Technol.*, *21(12)*, 1876–1894.

[4] Barth, A., Alvera-Azcrate, A.,Weisberg, R.H., 2008. Assimilation of high-frequency radar currents in a nested model of the West Florida Shelf. *J. Geophys. Res.*, 113, C08033, doi:10.1029/2007JC004585.

[5] Barth, A., Alvera-Azcrate, A., Beckers, J.M., Staneva, J., Stanev, E., Schulz-Stellenfleth, J., 2010: Correcting surface winds by assimilating High-Frequency Radar surface currents in the German Bight. *Ocean Dynamics*, 61, 599-610.

[6] A. Barth, A. Alvera-Azcrate, K.-W. Gurgel, J. Staneva, A. Port, J.-M. Beckers, and E. V. Stanev, 2010: Ensemble perturbation smoother for optimizing tidal boundary conditions by assimilation of High-Frequency radar surface currents - application to the German Bight. *Ocean Science*, 6(1), 161178, doi: 10.5194/os-6-161-2010.

[7] Beckers, J.M. and M. Rixen, 2003: EOF calculations and data filling from incomplete oceanographic observations, *J. Atm. Oceanic Tech.*, 20(12),1839-1856.

[8] Bennett, A.F., 2002: Inverse modeling of the ocean and atmosphere. Cambridge University Press, 256 pp

[9] Breivik, O., and O. Sætra, 2001: Real time assimilation of HF radar currents into a coastal ocean model, *J. Marine Sys.*, 28, 161-182.

[10] Chapman, R. D., L. K. Shay, H. C. Graber, J. B. Edson, A. Karachintsev, C. L. Trump, and D. B. Ross, 1997: On the accuracy of the HF radar surface measurements: Intercomparisons with ship-based sensors. *J. Geophys. Res.*, 102, 18,737-18,748.

[11] C. Chavanne, I. Janekovic, P. Flament, P.-M. Poulain, M. Kuzmic, and K.-W. Gurgel, 2007: Tidal currents in the northwestern Adriatic: High-frequency radar observations and numerical model predictions, *J. Geophys. Res.*, 112, C03S21, doi:10.1029/2006JC003523.

[12] Devenon, J-L., 1990: Optimal control theory applied to an objective analysis of a tidal current mapping by HF Radar. *J. Atmosph. Oceanic Tech.*, 7, 269-284.

[13] Eremeev, V.N., L.M.Ivanov and A.D. Kirwan, 1992: Reconstruction of oceanic flow characteristics from quasi-Lagrangian data: 1. Approach and mathematical methods. *J. Geophys. Res.*, 97(C6), 9733-9742.

[14] Fang, F., C.C. Pain, I. M. Navon, M.D. Piggott, G.J. Gorman, P.E. Farrell, P.A. Allison, and A.J.H. Goddard, 2008. A POD reduced-order 4D-var adaptive mesh ocean modelling approach, *Int. J. Num. Methods in Fluids*, doi:20.2002/fld.1911.

[15] Forget, P., Y. Barbin, and G. Andre, 2008: Monitoring of surface ocean circulation in the Gulf of Lions (North-West Mediterranian Sea) using WERA HF radars, *Proc. IGARSS*, CD ROM, Boston, USA (7-11 July).

[16] Graber, H. C., D. R. Thompson, and R. E. Carabde, 1996: Ocean surface features and currents measured with synthetic aperture radar interferometry and HF radar, *J. Geophys. Res.*, 101(C11), 25,813-25,832.

[17] Hisaki, Y., T. Tokeshi, W. Fujie, K. Sato, and S. Fujii, 2001: Surface current variability east of Okinawa Island obtained from remotely sensed and in situ observational data, *J. Geophys. Res.*, 106(C12), 31,057-31,073.

[18] Hodur, R. M., J. Pullen, J. Cummings, J., X. Hong, J.D. Doyle, P.J. Martin, M.A.Rennick, 2002: The coupled ocean-atmospheric mesoscale prediction system (COAMPS), *Oceanography*, 15(1), 88-98.

[19] Hoteit, I., B. Cornuelle, S.Y. Kim, G. Forget, A. Kohl and E. Terrill, 2009: Assessing 4D-VAR for dynamical mapping of coastal high-frequency radar in San Diego, *Dyn. Atmosph. Oceans*, 48, 175-197.

[20] Kaplan, D., and F. Lekien, 2007: Spatial interpolation of surface current data based on open-boundary modal analysis. *J. Geophys. Res.*, 112, C12007, doi: 10.1029/2006JC003984.

[21] Kim,S. Y., E. Terrill, and B. Cornuelle, 2007. Objectively mapping HF radar-derived surface current data using measured and idealized data covariance matrices, *J. Geophys. Res*, 112, C06021, doi:10.1029/2006JC003756.

[22] Kim,S. Y., E. Terrill, and B. Cornuelle, 2008. Mapping surface currents from HF radar radial velocity measurements using optimal interpolation, *J. Geophys. Res*, 113, C10023, doi:10.1029/2007JC004244.

[23] Kondrashov, D. and M. Ghil, 2006: Spatio-temporal filling of missing points in geophysical data sets, *Nonlin. Processes Geophys.*, 13, 151-159.

[24] Kurapov, A. L., G.D. Egbert, J.S. Allen, and R.N. Miller, 2009: Representer-based analyses in the coastal upwelling system, *Dyn. Atmosph. Oceans*, 48, 198-218.

[25] Kurapov, A.L., G.D. Egbert, J. S. Allen, R. N. Miller, S.Y. Erofeeva, P. M. Kosro, 2003: The M2 Internal Tide off Oregon: Inferences from Data Assimilation. *J. Phys. Oceanogr.*, 33, 17331757.

[26] Lekien, F., and C. Coulliette, 2004: Open-boundary modal analysis: Interpolation, extrapolation and filtering. *J. Geophys. Res.*, 109, C12004, doi:10.1029/2004JC002323.

[27] Le Provost C. and A. Poncet, 1978: Finite element method for spectral modelling of tides. *Int. J. Num. Meth. in Engineer.*, 12, 853-871.

[28] Lewis, J.K., I. Shulman, and A.F. Blumberg, 1998: Assimilation of the Doppler radar current data into numerical ocean models, *Cont. Shelf Res.*, 18, 541-559.

[29] Li, Z., Y. Chao, J.C. McWilliams, and K. Ide, 2009: A three-dimensional variational data assimilation scheme for the Regional Ocean Modeling System, *J. Atmosph. Oceanic Tech.*, 25, 2074-2090.

[30] Lipa, B.J., and D.E. Barrick, 1983: Least-squares methods for the extraction of surface currents from CODAR crossed-loop data: Application at ARSLOE *IEEE J. Ocean. Eng.*, 8(4), 226253.

[31] Lipa, B., Nyden, B., Ullman, D.S., and Terrill, E., 2006: SeaSonde radial velocities: derivation and internal consistency. *IEEE J. Oceanic Eng.*, 31(4), 850-861.

[32] Lipphardt, B. L., A. D. Kirwan, C. E. Grosch, J. K. Lewis, and J. D. Paduan, 2000. Blending HF radar and model velocities in Monterey Bay through normal mode analysis. *J. Geophys. Res.*, 105, C2, 3,425-3,450.

[33] Mariette, V., N. Thomas, V. Cochin, Y. Guichoux, and F. Ardhuin, 2006: Premiers résultats de lexpérience SURLITOP (Surveillance Littorale Opérationnelle), *Navigation*, 54, 4557.

[34] McIntosh, P. C., 1990. Oceanographic data interpolation: Objective analysis and splines. *J. Geophys. Res.*, 95(C8), 13,529-13,541.

[35] Oke, P.R., Allen, J.S. Miller, R.N., and Egbert G.D. 2002: A modelling study of the three-dimensional continental shelf circulation off the Oregon. Part I. Dynamical analysis. *J. Phys. Oceanogr.*, 32, 1383-1403. *J. Geophys. Res*. 109, C07S09.

[36] Oke, P.R., Allen, J.S., Miller, R.N., Egbert, G.D., Kosro, P.M., 2002: Assimilation of surface velocity data into a primitive equation coastal ocean model. *J. Geophys. Res.*, doi:10.1029/2000JC00511.

[37] Oke, P., Allen, J, Miller, R., Egbert, G., Kosro, P., 2010. Assimilation of surface velocity data into a primitive equation coastal ocean model. *Ocean Dynamics*, 60, 1497-1537.

[38] Paduan, J.D., Shulman, I., 2004: HF radar data assimilation in the Monterey Bay area. *J. Geophys. Res*. 109, C07S09.

[39] Park, K., Z. Li, J. Farrara and Yi Chao, 2007: Assimilation of high-frequency radar measurements for coastal currents using ROMS, *Proc. SPIE*, vol. 6685, doi:10.1117/12.759504, 55-68.

[40] Prandle, D., 1993: Year-long measurements of flow through the Dover Strait by HF radar, *Oceanologica Acta*, 16, 457-468.

[41] Sentchev, A. and M. Yaremchuk, 1999: Tidal motions in the Dover Straits as a variational inverse of the sea level and surface velocity data, *Cont. Shelf Res.*, 19, 1905-1932.

[42] Sentchev, A., M. Yaremchuk, and F. Lyard 2006: Residual circulation in the English Channel as a dynamically consistent synthesis of shore-based observations of sea level and currents, *Cont. Shelf Res.*, 26, 1884-1904.

[43] Sentchev, A. and M. Yaremchuk, 2007: VHF radar observations of surface currents off the northern Opal coast in the eastern English Channel, *Cont. Shelf Res.*, 27, 2449-2464.

[44] Sentchev, A., P. Forget, Y. Barbin, and M. Yaremchuk, 2012: Surface circulation in the Iroise Sea (Western Brittany) derived from high resolution current mapping by HF radars. *J. Marine Systems* (in press).

[45] Shay, L. K., J. Martinez-Pedala, T. M. Cook, and B. K. Haus, 2007: High-frequency radar mapping of surface currents using WERA. *J. Atm. Oceanic Tech.*, 24, 484-503.

[46] Shulman, I.,Wu, C.R., Lewis, J.K., Paduan, J.D., Rosenfeld, L.K., Kindle, J.C., Ramp, S.R., Collins, C.A., 2002. High resolution modeling and data assimilation in the Monterey Bay area. *Cont. Shelf Res.* 22(8), 11291151.

[47] Shulman, I., Kindle, J., Martin, P., deRada, S., Doyle, J., Penta, B., Anderson, S., Chavez, F., Paduan, J., Ramp, S., 2007. Modeling of upwelling/relaxation events with the Navy Coastal Ocean Model. *J. Geophys. Res.* 112, C06023, doi:10.1029/2006JC003946.

[48] Shulman, I. and J. Paduan, 2009. Assimilation of HF radar-derived radials and total currents in the Monterrey Bay area, *Deep-Sea Res. II*, 56, (3-5), 149-160.

[49] Tipett, M.K., J. Anderson, C. Bishop, T. M. Hamill and J. S. Whitaker, 2003: Ensemble square root filters. *Mon. Wea. Review*, 131, 1485-1490.

[50] Wilkin, J.L., H.G. Arango, D.B. Haidvogel, C.S. Lichtenwalner, S.M. Glenn, and H.S. Hedstrm, 2005: A Regional Ocean Modeling System for the long-term ecosystem observatory. *J. Geophys. Res*, 110, C06S91.

[51] Yaremchuk, M., and A. Sentchev, 2009: Mapping radar-derived sea surface currents with a variational method, *Cont. Shelf Res.*, 29, 1711-1722.

[52] Yaremchuk, M., D. Nechaev, and G. Panteleev, 2009: A method of successive corrections of the control subspace in the reduced-order variational data assimilation, *Mon. Wea. Rev.*, 137(9), 2966-2978.

[53] Yaremchuk, M., , and A. Sentchev, 2011: A combined EOF/variational approach for mapping radar-derived sea surface currents, *Cont. Shelf Res.*, 31, 758-768.